*inorganics*

MDPI

*Article*

# A Manganese(II) 3D Metal–Organic Framework with Siloxane-Spaced Dicarboxylic Ligand: Synthesis, Structure, and Properties

**Alexandru-Constantin Stoica [1], Madalin Damoc [1], Sergiu Shova [1], Ghenadie Novitchi [2], Mihaela Dascalu [1,*] and Maria Cazacu [1,*]**

[1] Department of Inorganic Polymers, "Petru Poni" Institute of Macromolecular Chemistry, Aleea Grigore Ghica Voda 41A, 700487 Iasi, Romania
[2] Laboratoire National des Champs Magnétiques Intenses (LNCMI) Université Grenoble Alpes, INSA Toulouse, Université Toulouse Paul Sabatier, EMFL, CNRS, F-38042 Grenoble, France
* Correspondence: amihaela@icmpp.ro (M.D.); mcazacu@icmpp.ro (M.C.)

**Abstract:** A new metal–organic framework $\{[Mn_4(Cx)_3(etdipy)_5]\cdot 2ClO_4\}_n$ (**1**) was prepared via the complexation of manganese ion from a $Mn(ClO_4)_2$ source with 1,3-bis(carboxypropyl) tetramethyldisiloxane (Cx) and 1,2-di(4-pyridyl)ethylene (etdipy) in the presence of 2,4-lutidine as a deprotonating agent. The single-crystal X-ray diffraction analysis revealed a dense 3D framework structure. The presence in the structure of flexible tetramethyldisiloxane moieties, which tend to orient themselves at the interface with the air, gives the compound a highly hydrophobic character, as indicated by the result of the water vapor sorption analysis in the dynamic regime, as well as the shape and stability of the water droplet on the crystalline mass of the compound. The compound is an electrical insulator, and due to its hydrophobicity, this characteristic is unaffected by environmental dampness. The thermal analysis indicated thermal stability up to about 300 °C and an unusual thermal transition for an MOF structure, more precisely a glass transition at 24 °C, the latter also being attributed to the flexible segments in the structure. The magnetic studies showed dominant antiferromagnetic interactions along the metal ion chain in compound **1**.

**Keywords:** siloxane moiety; carboxylate ligand; manganese(II); 3D MOF; magnetic properties



**Citation:** Stoica, A.-C.; Damoc, M.; Shova, S.; Novitchi, G.; Dascalu, M.; Cazacu, M. A Manganese(II) 3D Metal–Organic Framework with Siloxane-Spaced Dicarboxylic Ligand: Synthesis, Structure, and Properties. *Inorganics* **2023**, *11*, 21. https://doi.org/10.3390/inorganics11010021

Academic Editor: Claudio Pettinari

Received: 15 December 2022
Revised: 26 December 2022
Accepted: 29 December 2022
Published: 1 January 2023



## 1. Introduction

Metal–organic frameworks (MOFs) are porous polymeric coordination structures built from the assembly of inorganic sub-units (a single metal center, a cluster, or a chain) and organic linkers of various types (carboxylates, phosphonates, azolates, etc.); there are numerous options for altering the precursors' characteristics and combinations of those precursors, enabling the precise adjustment of the final material's structure and properties. A number of factors, including the connectivity of the organic building blocks, coordination geometry of metal ions, reaction temperatures, solvents, pH, and presence of auxiliary ligands, may have an impact on the outcomes [1–6]. Due to their extreme porosity and stiffness, which result in intriguing features and possible uses, these materials are of tremendous interest [7] in a variety of fields, including gas storage [8], gas capture [9], molecular sensing [10], separation [11], and catalysis [12]. Although the high absorption capabilities of porous MOFs are well known, different functionalities (such as magnetic [13], electrical [14], or optical [15]) can be added to them by carefully selecting the functional nodes and organic linkers and choosing how they relate to one another, or by including functional molecules in the pores. Polycarboxylic acids, generally the rigid aromatic ones (terephthalic, isophthalic, trimesic, etc.) and pyridyl derivatives, are the ligands most widely approached for the construction of MOFs to ensure their porosity, stability, and crystallinity [16–20], while monocarboxylic ligands are more suitable for building clusters. In the case of manganese

complexation, for example, with monocarboxylic acids, clusters capable of functioning as single molecular magnets (SMM) were obtained [21–23]. Manganese complexes with carboxylic ligands have been widely studied, with the literature providing a significant volume of structural data on such complexes, due to the structural diversity (both chemical and magnetochemical) generated by the varied nuclearity (from Mn1 to Mn18) and the mode of coordination of the carboxylate ions (e.g., monodentate–bidentate, bridging–terminal, syn–anti). Most of these structures are obtained either directly via self-assembly, often using additional ligands or polycarboxylic acids, or by using preformed clusters [24,25].

Unlike the widely studied MOFs based on rigid ligands, MOFs based on flexible ligands are much less addressed, although they too could present some interesting behaviors [26]. On the one hand, the conformational flexibility of the ligand can either facilitate the manifestation of most of the possible supramolecular interactions, and as a result the formation of a structure with low porosity, or on the contrary it can allow the formation of large pores, which may collapse during the activation process. Therefore, the BET surface area and actual sorption capacity values are often found to be much lower than the theoretical estimates. This is why efforts are being made to limit this shortcoming or to find areas of application for which this peculiarity is of interest, such as for proton conduction [27–30] or for carbonization leading to highly porous carbons [16,31,32].

In recent years, we have used a dicarboxylic acid with a long and flexible spacer, 1,3-bis(carboxypropyl)tetramethyldisiloxane (Cx), as a ligand to obtain coordination polymers of various metals (Cu, Co, Mn, or Zn as the acetate or perchlorate) of the 1D [33] or 2D type, in the latter case in the presence of co-ligands based on nitrogen heterocycles (4,4′-azopyridines [34,35], imidazole [35,36], or derivatives of bipyridyl [37]), often in the presence of a small amount of lutidine as a deprotonating agent. In this manuscript, we report for the first time a 3D structure based on Mn with this ligand and 1,2-di(4-pyridyl)ethylene (etdipy) by slightly changing the reactant ratio. The structure is identified using a single-crystal X-ray diffraction analysis supported by spectral and elemental analyses. The compound is evaluated from the point of view of the surface, thermal, and magnetic behaviors.

## 2. Results

The reaction of $Mn(ClO_4)_2$ with Cx and etdipy in the presence of 2,4-lutidine, as depicted in Scheme 1, led to a complex structure **1**, as 2D yellow crystals.

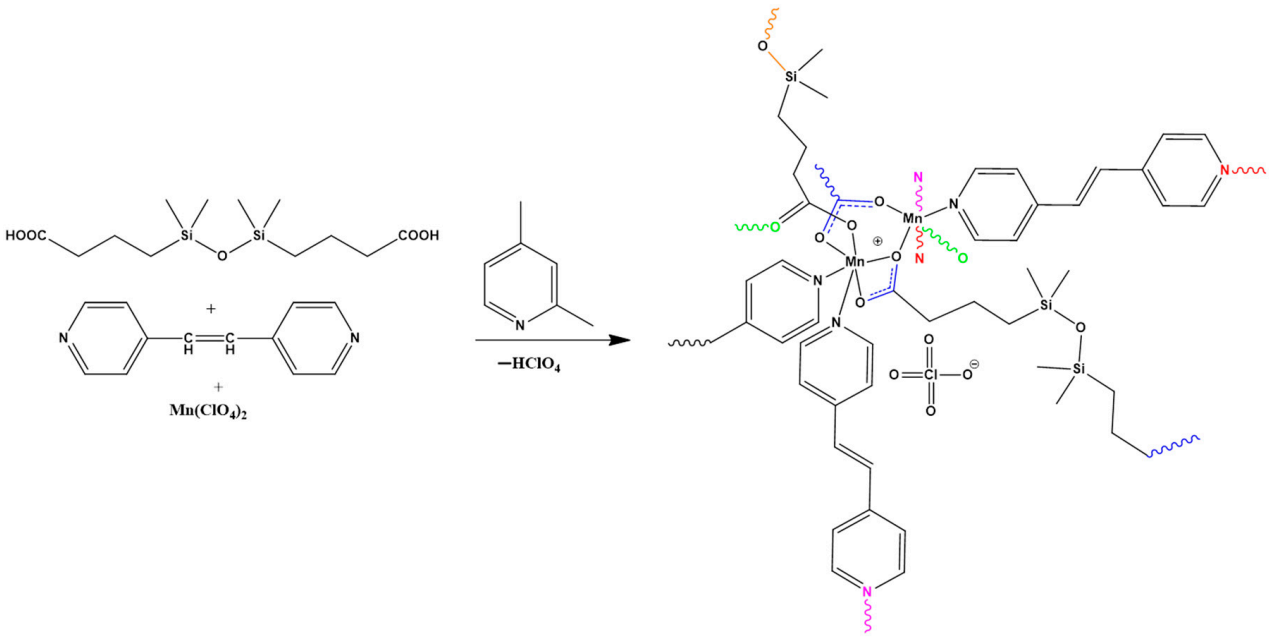


**Scheme 1.** The reaction leading to the 3D coordination polymer **1**.

### 2.1. FTIR Spectroscopy

The spectrum variations of the molecule (Figure S1) in comparison to the starting compounds provide the first cues about the formation of complex **1**, namely the disappearance of the absorption band characteristic to the carboxyl group from 1709 $cm^{-1}$ and the appearance of bands from 1547 and 1427 $cm^{-1}$, assigned to the $\nu_{as}(COO^-)$ and $\nu_s(COO^-)$ vibration bands in carboxylate, respectively. The analysis revealed the presence of asymmetric and symmetric stretching and deformation bands characteristic of tetramethyldisiloxane fragments (837 $cm^{-1}$ (C–H from *Si–CH*$_3$ stretching), 1090 (*Si–O–Si* stretching), and 1252 (C–H deformation in *Si–CH*$_3$)) and the band specific to nitrogen atoms from the aromatic ring (1609 $cm^{-1}$). Since a split signal appears in the 1590–1515 $cm^{-1}$ region, the area characteristic of the asymmetric carboxylate band, the IR spectrum was deconvoluted, with three bands characteristic of the carboxylate groups being highlighted. The bands from 1546 and 1430 $cm^{-1}$ are assigned to the chelated carboxylate group, and those from 1572 and 1449 $cm^{-1}$ bands correspond to the bridged carboxylate group, while those from 1564 and 1412 $cm^{-1}$ correspond to a possible bridged or monodendate carboxylate group based on the difference of $\upsilon_{as}(COO^-)$—$\upsilon_s(COO^-)$ (carboxyl-end group polymer) (Figure 1). The $\upsilon_{as}(COO^-)$ and $\upsilon_s(COO^-)$ bands corresponding to the Na salt appear at 1566 and 1414 $cm^{-1}$, respectively. Considering these aspects, based on the IR analysis, a structure can be proposed in which the metal atoms present a chelated and bridge-type environment (with the possibility of a second type of bridging; see the next X-ray section for details). The obtained results are consistent with similar data from the literature [38,39]. The interpretation based on the IR data is sustained by the single-crystal X-ray analysis.

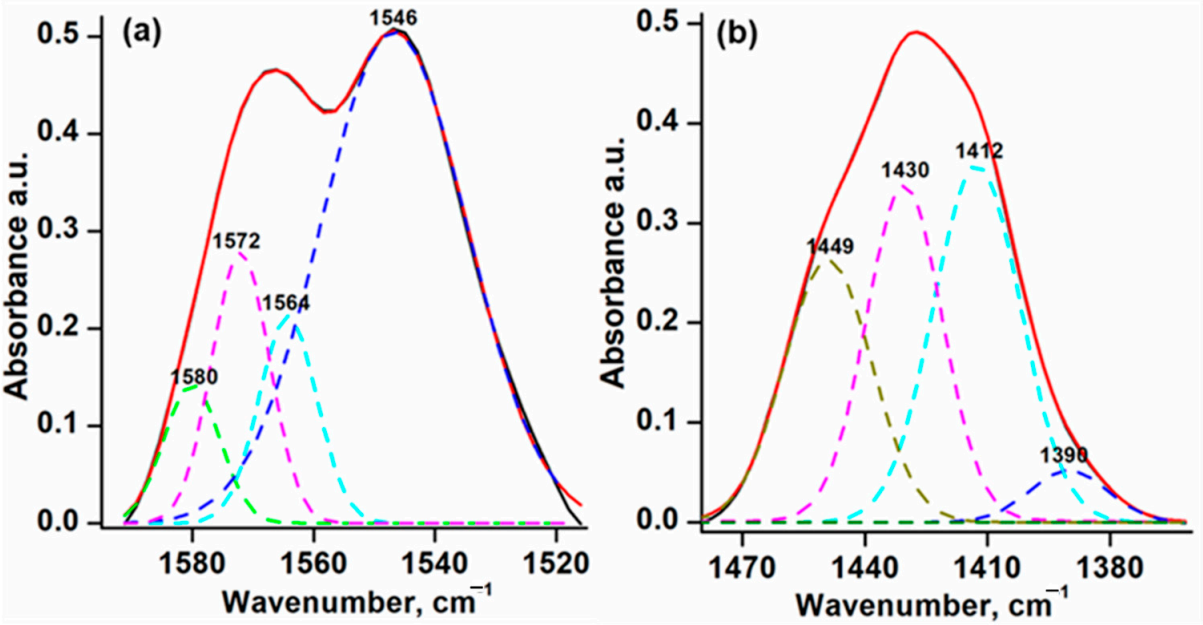


**Figure 1.** The deconvoluted IR spectra in the 1515–1595 $cm^{-1}$ (**a**) and 1360–1480 $cm^{-1}$ (**b**) carboxylate band region of polymer **1**.

### 2.2. X-ray Crystallography

The single-crystal X-ray diffraction analysis revealed compound **1** to be built from cationic 3D coordination polymers and $ClO_4^-$ anions. The asymmetric unit (Figure 2) comprises two $Mn^{2+}$ ions in the general positions, 1.5 double deprotonated ligands $(Cx)^{2-}$, 2.5 etdipy molecules, and one perchlorate counter-anion. The eight positive chargers from four Mn(II) ions are counterbalanced by eight negative charges from three deprotonated $Cx^{2-}$ ligands and two $ClO_4^-$ out-of-sphere anions, so that the charge balance is in agreement with the formation of $\{[Mn_4(Cx)_3(etdipy)_5]\cdot 2ClO_4\}_n$ species.

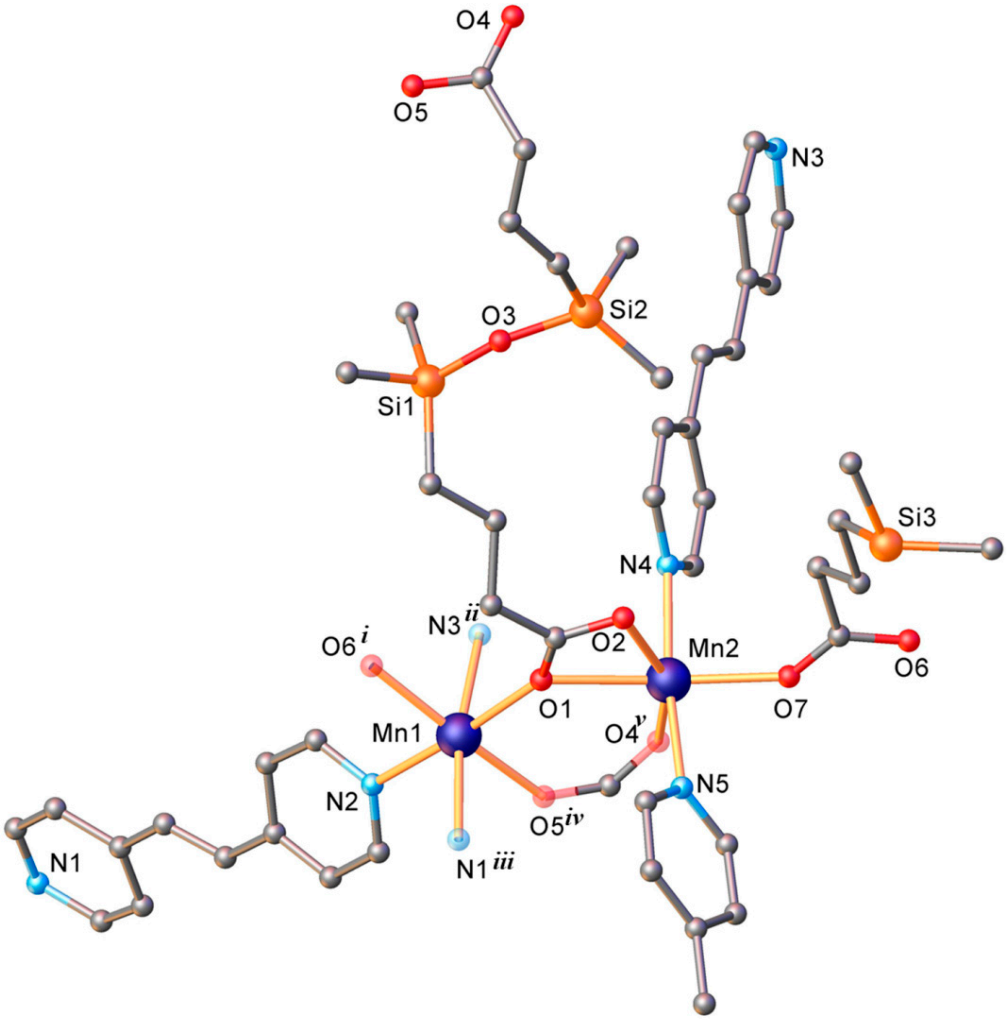


**Figure 2.** View of the asymmetric part showing the coordination of the Mn(II) atoms in compound **1**. The out-of-sphere $ClO_4^-$ atoms are not shown. The symmetrical atoms are drawn with faded colors. Symmetry codes: $^{(i)}$ $1-x, 1-y, -z$; $^{(ii)}$ $x, 1/2-y, 1/2-z$; $^{(iii)}$ $-x, -1/2+y, 1/2-z$; $^{(iv)}$ $-1+x, 1/2-y, -1/2+z$; $^{(v)}$ $-1+x, 1/2-y, -1/2+z$.

Both Mn(II) atoms are six-coordinated, but have different coordination geometries. The coordination polyhedron of Mn1 is described as a slightly distorted $N_3O_3$ octahedron. As for Mn2, considering that the three dentate-bridging carboxylate groups occupy only one coordination position, it could be assumed that the coordination geometry is a distorted trigonal bipyramid.

The analysis of the structure also revealed that the carboxylate groups fulfill three different bridging structure functions, being coordinated as *syn-syn* bidentate, *syn-anti* bidentate, and tridentate bridging ligands, which generate the formation of the one-dimensional array, as shown in Figure 3. The Mn1···Mn2 and Mn1···Mn2$^i$ separations within the 1D coordination polymer are at 5.7190(14) Å and 3.8556(13) Å, respectively. The further interconnection of 1D chains occurs through $Cx^{2-}$ and etdipy linkers to form a dense three-dimensional coordination network, as shown in Figure 4. The Mn···Mn separations across etdipy and Cx linkers are in the range of 13.9104(18) ÷ 13.9282(11) Å and 12.7381(19) ÷ 15.008(2) Å (Figures S2 and S3), respectively. The presence of the π-π stacking interaction (Figure 5), which is evidenced by the short centroid-to-centroid distance of 3.67516(14) Å between the centro-symmetrically related etdipy units, is also noted.

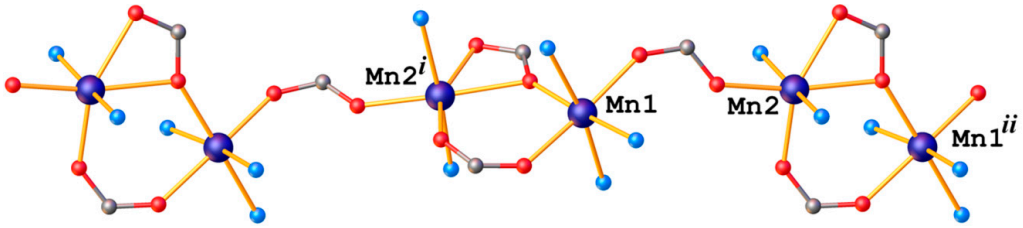


**Figure 3.** The 1D arrangement of metal ions, highlighting the coordination functions of the carboxylate groups. Symmetry codes: $^{(i)}$ $x$, $1/2 - y$, $-1/2 + z$; $^{(ii)}$ $x$, $1/2 - y$, $1/2 + z$.

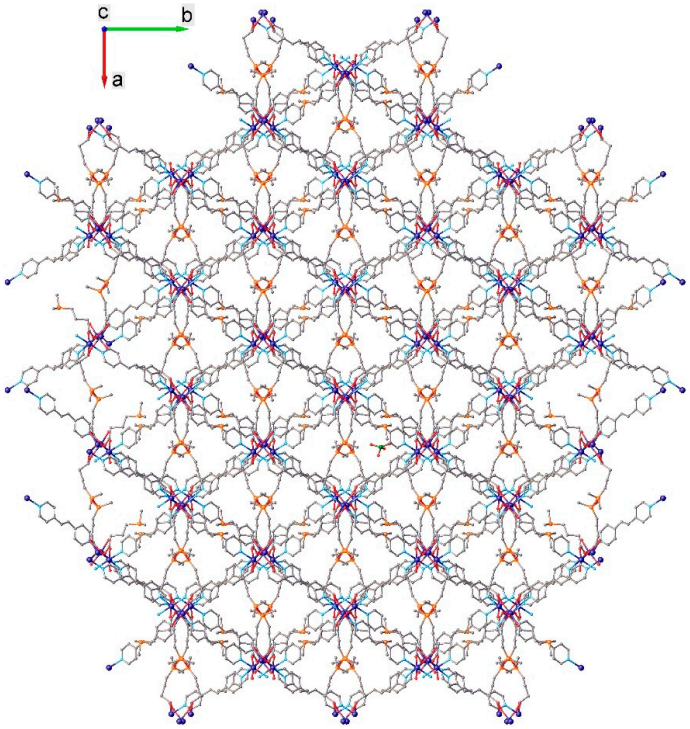


**Figure 4.** The crystal structure of compound **1**.

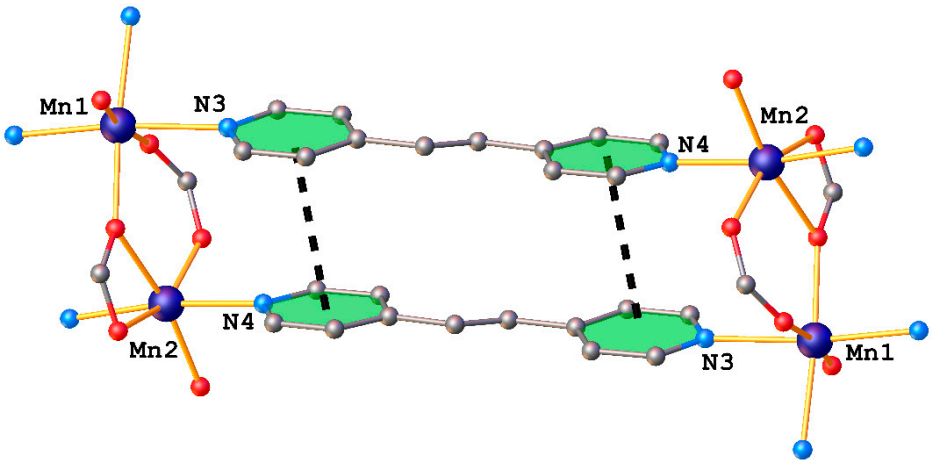


**Figure 5.** The fragment of the 3D coordination network showing π-π interactions in compound **1**.

The high density of the above-mentioned 3D network, along with the presence of $ClO_4^-$ out-of-sphere counter-anions and statistically disordered highly flexible siloxane fragments, facilitate a drastic reduction in the solvent-accessible areas in the crystal, while according to the Mask routine, those accessible in Olex2 represent less than 2.3%. The

BET surface estimated on the basis of nitrogen sorption isotherms is extremely low, at 0.478 $m^2/g$. According to the ToposPro [40] analysis (Figure S4), the bitopic ligands Cx and etdipy coordinated to Mn(II) ions generate a new type of three-periodic net that is 4-nodal net connected with (4-c)2(4-c)(5-c)2(6-c)2 stoichiometry and point symbols $\{4.5^2.6^3.7^3.8\}_2\{4.5^3.6^5.7^5.8\}_2\{4^2.5^2.7^2\}_2\{5^3.6^2.7\}$.

### *2.3. Hydrophobic Behaviour*

Since the MOFs' sensitivity to moisture restricts their practical application in some domains, hydrophobicity is a desired property for MOFs generally. MOFs that maintain their integrity after longer storage lengths can be obtained using three-dimensional stiff shielding ligands [41]. Using Cx as a ligand, the dimethylsiloxane moieties' high flexibility (Si-O bond length and Si-O-Si angle) [42–45], the long bond length of Si-$CH_3$ (1.7–1.9Å), and the incapability of $CH_3$ groups to create intermolecular physical interactions because of their extremely non-polar character [46] result in the latter migrating and densely packing the material's surface, providing it with surface hydrophobicity.

The dynamic water vapor sorption results and optical images (Figure 6) evidenced the hydrophobic behavior of compound **1**. The water sorption–desorption dynamic analysis indicated a sorption capacity of 1.4% at room temperature, with a BET area of 13.17 $m^2/g$ (calculated with the IGA sorption device software), higher than that estimated based on the sorption of larger and non-polar nitrogen molecules. The final mass of the sample, after the sorption–desorption cycle, is not the same with the initial one because some of the sorbed water remains in the sample. The rolling of the water drop on the compound's surface, entrapping material particles on the surface, sustains the hydrophobicity of the tested compound. When the material's roof collapses, the drop maintains its spherical shape until all of the water has evaporated [47]. Rolling water droplets imply a contact angle >150°, which equates to a superhydrophobic substance according to the literature reports [48]. The attachment of the material particles to the water drop's surface and their persistence during its rolling, however, point to a paradoxical occurrence that might be related to the *petal effect*—a very sticky superhydrophobicity [49,50]. Instead, the oil quickly covers the entire mass of the material on which the drop was deposited.

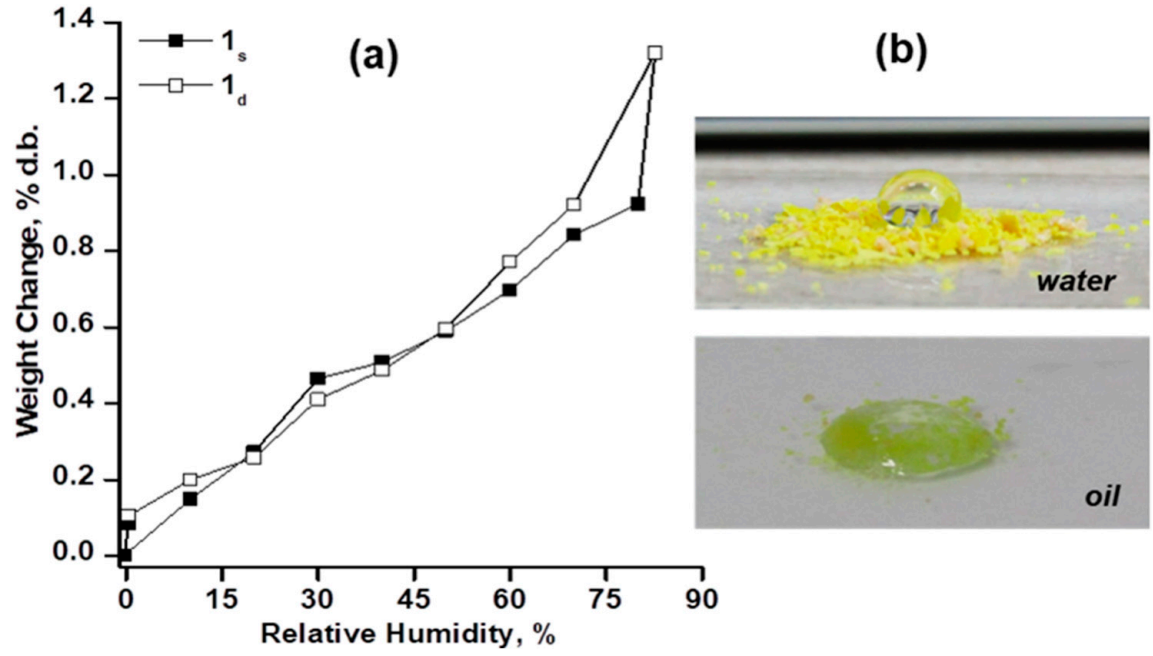


**Figure 6.** The moisture sorption–desorption isotherms for compound **1**, where the *s* and *d* subscript coefficients represent the sorption and desorption isotherms (**a**). Optical images of the water and oil droplets on compound **1** indicating hydrophobic behavior (**b**).

### *2.4. Thermal and Dielectric Behaviors*

The thermogravimetric analysis was conducted to evaluate the thermal stability of compound **1** at a heating rate of 10 °C $min^{-1}$ (Figure 7). The thermogravimetric curve presents three weight loss steps. The first weight loss registered below 100 °C of only 1% corresponds to the desorption of physically absorbed water and remaining solvents. The second weight loss, which is the main one, of about 43% in the 300 °C ÷ 350 °C temperature range, is attributed to the thermal decomposition of the ligand. The last stage of weight loss of 17% in the 390 ÷ 700 °C range is attributed to the decomposition of the Si-O-Si structure and metal-based moiety with the formation of $SiO_2$ and MnOx.

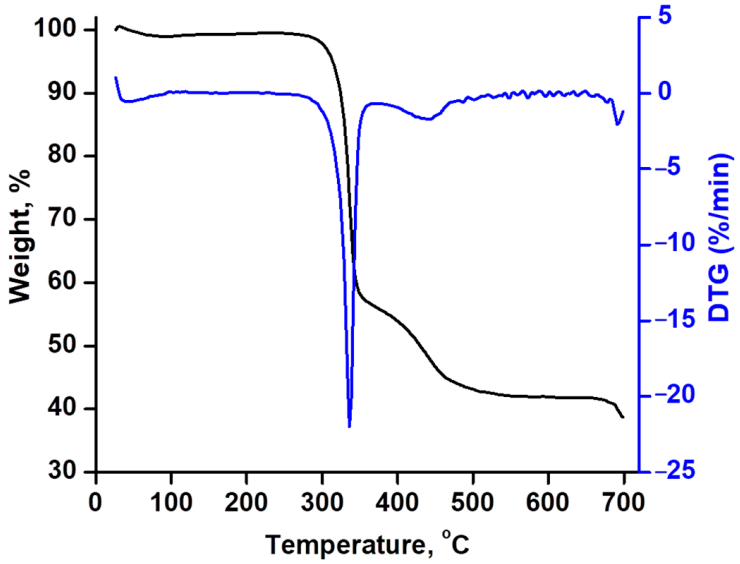


**Figure 7.** Thermogravimetric analysis of compound **1**.

The DSC traces for compound **1** in the range of −150 ÷ +150 °C reveal the presence of a glass transition at 24.34 °C (Figure 8), which is unusual for an MOF and is assigned to the tetramethyldisiloxane spacer from the Cx ligand, which makes up the amorphous part of the structure and is highly flexible and unable to form meaningful intermolecular connections. The glass transition is influenced by the presence of hydrogen bonds [51]. Methylsiloxane substrates are characterized by very low glass transition temperatures due to their inability to form hydrogen bonds; hence, the increase in *Tg* is attributed totally to the attached polar groups, namely −COOH or C=O, which are capable of forming such bonds.

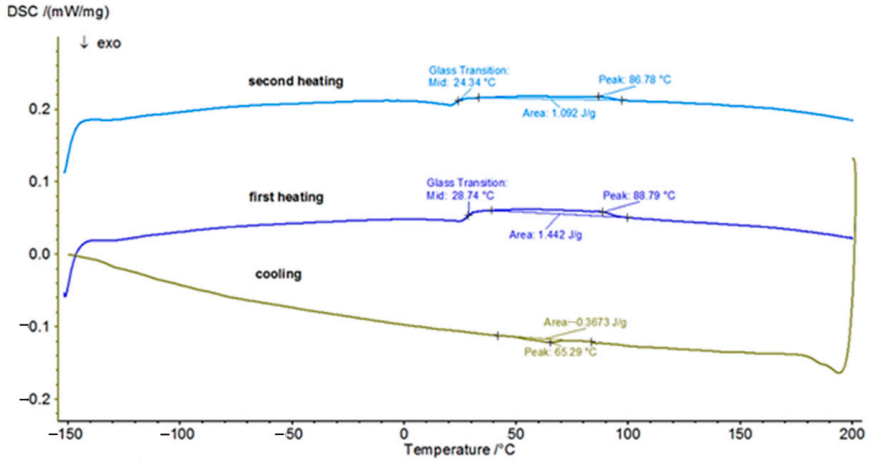


**Figure 8.** The DSC curves for compound **1**.

Being that this study is about a compound that contains metal in structure, we had the idea to investigate the electrical properties. The results indicate an insulating material ($\sigma = 10^{-14} \div 10^{-8}$ S/cm) with an almost constant dielectric permittivity value ($\varepsilon' \approx 3$) throughout the studied frequency range ($10^0 \div 10^6$ Hz) under normal temperature and humidity conditions. When the humidity reaches 80% RH, the conductivity is unaffected but a slight increase in permittivity is shown (Figure S5).

### *2.5. Magnetic Properties*

The temperature dependence of the magnetic susceptibility of the polymer chain was measured in the temperature range of $2 \div 300$ K under a magnetic field of 0.1 T (Figure 9). At room temperature (300 K), the χT value per Mn(II) is 4.267 $cm^3$ $mol^{-1}$ K, which is slightly lower than theoretically expected for the magnetically decoupled Mn(II) ion (S = 5/2, 4.375 $cm^3$ $mol^{-1}$ K, assuming g = 2.0) [52]. Upon cooling, the product of χT gradually decreases and reaches a value equal to 0.307 $cm^3$ $mol^{-1}$ K at 2 K. Such behavior suggests the presence of a dominant antiferromagnetic interaction along the chain. The magnetization curves measured at T = 2, 3, 4, and 5 K with the applied magnetic field varying from 0 to 5 T show the linear dependence of the magnetization (Figure S6), which is characteristic of the presence of an antiferromagnetic interaction.

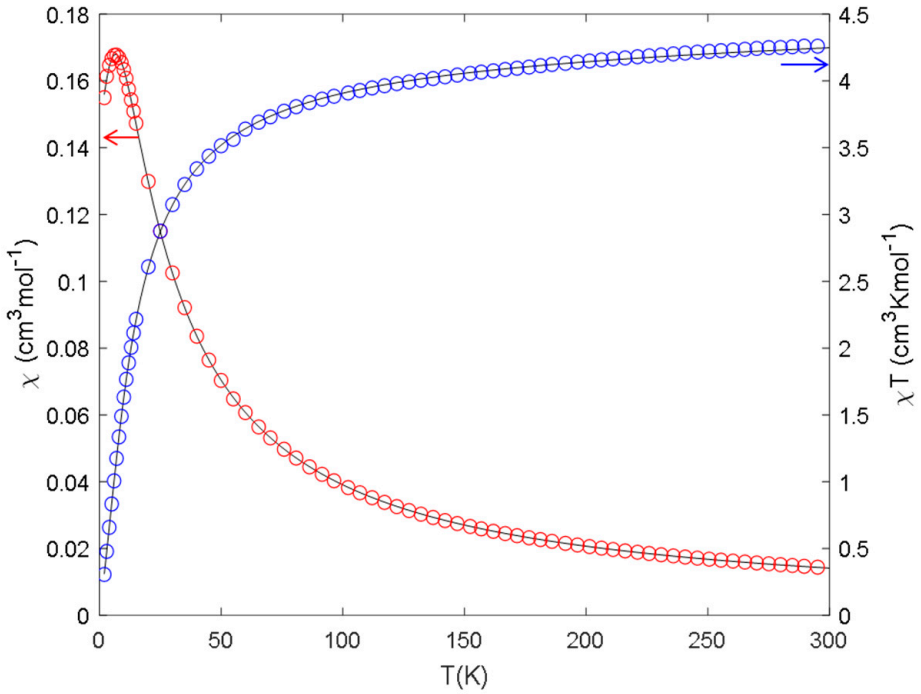


**Figure 9.** Thermal variations in the magnetic susceptibility (χ) and χT product for compound **1**. The solid line represents the best fit according to the model.

According to the single-crystal X-ray diffraction analysis, the polymer consists of 1D chains of Mn(II) ions alternately linked by two and one carboxylic ligand (Figure 3). For the alternating chains of isotropic spins $S_i = 5/2$, the following model was proposed based on the Hamiltonian function [53]:

$$H = -J_1 \sum S_{2i} S_{2i+1} - J_2 \sum S_{2i+1} S_{2i+2} \quad (1)$$

The exchange parameters $J_1$ and $J_2$ reflect the magnetic couplings between the Mn(II) ions via the bridging carboxylate ligands. The numerical expression for the temperature variation of the magnetic susceptibility that derives from the Hamiltonian function (Equation (1)) is presented in the Supporting Information.

The best-fitting parameters obtained were $J_1$ = −1.69(1) K, $J_2$ = −0.64(1) K, and g = 2.009(3), which are represented as solid lines in Figure 9. The obtained values correspond to the two types of bridging in the chain. Both magnetic interactions are antiferromagnetic, with $J_1$ probably reflecting the interaction through two carboxylic groups and $J_2$ for the bridge made through a single carboxylic bridge. Similar models have been applied for different alternated Mn(II) 1D polymeric chains [54–56]. It is known that the magnetic interaction with Mn(II) through carboxylates is always small and depends on the coordination mode and conformation of the bridging carboxylate groups [57–60].

## 3. Materials and Methods

### *3.1. Materials*

The 1,3-bis(carboxypropyl)tetramethyldisiloxane, Cx, $C_{12}H_{10}N_2$, M = 306.51 g/mol (Gelest, Inc., Bucks County, PA, USA); 1,2-di(4-pyridyl)ethylene, etdipy, M = 182.22 g/mol (Aldrich); 2,4-lutidine, M = 107.15 g/mol, (Aldrich); and $Mn(ClO_4)_2$, methanol, and ethylic ether were purchased from Aldrich.

### *3.2. Methods of Characterization*

The Fourier transform infrared (FTIR) spectra in transmission mode (400–4000 $cm^{-1}$ spectral range, 2 $cm^{-1}$ resolution, with the accumulation of 32 scans, room temperature) were recorded on a Bruker Vertex 70 FT-IR spectrometer. The carbon, hydrogen, and nitrogen contents were determined on a Perkin–Elmer CHNS 2400 II elemental analyzer. The single-crystal X-ray diffraction measurements were carried out with an Oxford-Diffraction XCALIBUR E CCD diffractometer equipped with graphite-monochromated MoKα radiation. The single crystals were positioned at 40 mm from the detector and 330 frames were measured for 200 s over a 1° scan width for compound **1**. The unit cell determination and data integration processes were carried out using the CrysAlis package from Oxford Diffraction [61]. The structures were solved by Intrinsic Phasing using Olex2 [62] software with the SHELXT [63] structure solution program and refined by full-matrix least-squares on *F2* with SHELXL-2015 [64] using an anisotropic model for non-hydrogen atoms. All H atoms were introduced in idealized positions ($d_{CH}$ = 0.96 Å). Table 1 gives the main crystallographic data with the refining details, while in Table S1 a selection of bond lengths, angles, and hydrogen bonds is provided. The powder X-ray diffraction analysis was performed on a Rigaku Miniflex 600 diffractometer using CuKα emission in the angular range of 2–50° (2θ), with a scanning step of 0.01° and a recording rate of 2°/min. The BET surface area was estimated from nitrogen sorption–desorption isotherms recorded on a Quantachrome NOVA analyzer. The moisture sorption behavior of the sample was studied in the dynamic regime at 25 °C, in the 0–90% relative humidity (RH) range, using an IGAsorp fully automated gravimetric analyzer fabricated by Hiden Analytical, Warrington (UK). The thermogravimetric analysis (TGA) was performed on a Mettler Toledo 851 derivatograph in a nitrogen atmosphere within a 29–800 °C temperature range. The differential scanning calorimetry (DSC) curves were recorded with a Mettler–Toledo DSC 1 system operating under nitrogen flow (150 mL/min) from 25 °C until reaching the stability limit of compound. The dielectric permittivity and conductivity were evaluated on the basis of the measurements recorded on a Novocontrol Concept 40 Broadband Dielectric Spectrometer device equipped with an Alpha-A High-Performance Frequency Analyzer, in a broad frequency range ($10^0 \div 10^6$ Hz) at room temperature. The *Dc* magnetic susceptibility data (2–300 K) were collected on powdered samples using a SQUID magnetometer (Quantum Design MPMS-XL), applying a magnetic field of 0.1 T. All data were corrected for the contribution of the sample holder and the diamagnetism of the samples estimated from Pascal's constants [52,65]. The field dependence of the magnetization (up to 5 T) was measured between 2.0 and 5.0 K. The fitting of the magnetic properties was carried out in MATLAB (R2021a) software based on the mathematical expressions presented in the Supporting Information.

**Table 1.** The crystal data and details of the data collection process.

| | |
|---|---|
| empirical formula | $C_{96}H_{122}Cl_2Mn_4N_{10}O_{23}Si_6$ |
| *Fw* | 2243.23 |
| space group | $P2_1/c$ |
| *a* [Å] | 15.9092(8) |
| *b* [Å] | 22.2710(6) |
| *c* [Å] | 17.8188(9) |
| α [°] | 90 |
| β [°] | 112.866(6) |
| γ [°] | 90 |
| *V* [Å$^3$] | 5817.3(5) |
| *Z* | 2 |
| $\rho_{calcd}$ [g·cm$^{-3}$] | 1.281 |
| crystal size [mm] | 0.15 × 0.09 × 0.05 |
| T [K] | 293(2) |
| $\mu$ [mm$^{-1}$] | 0.599 |
| 2Θ range | 3.444 to 50.054 |
| reflections collected | 35246 |
| independent reflections | 10185 [$R_{int}$ = 0.0743] |
| data/restraints/parameters | 10185/161/616 |
| $R_1$ | 0.0980 |
| $wR_2$ | 0.2706 |
| GOF | 1.020 |
| Largest diff. peak/hole [e·Å$^{-3}$] | 1.33/−0.74 |
| CCDC | 2222958 |

### *3.3. Procedure for the Synthesis of Coordination Polymer 1*

To a solution of 1,3-bis(carboxypropyl)tetramethyldisiloxane (0.1125 g, 0.3675 mmole) in MeOH (10 mL), a solution of 1,2-di(4-pyridyl)ethylene (0.066 g, 0.3675 mmole) in MeOH (5 mL) was added. The mixture was stirred at room temperature for 30 min, followed by the addition of 50 µL 2,4-lutidine with heating at reflux for 2 h. A solution of $Mn(ClO_4)_2$ (0.375 mmole) in $H_2O$ (5 mL) was added over the reaction mixture, which was again heated at reflux for 1 h and stirred at room temperature overnight. Then, the reaction mixture was allowed to slowly (ca. one month) evaporate the solvents, resulting in yellow rectangular plate crystals (suitable for the single-crystal X-ray diffraction analysis), which further were washed with water, methanol, and ethylic ether. The specific IR absorption bands were as follows (KBr, cm$^{-1}$): 3441 m, 3063 w, 2951 m, 2924 m, 2895 m, 1609 vs, 1566 vs, 1547 vs, 1503 m, 1427 s, 1315 w, 1252 s, 1223 m, 1169 w, 1103 vs, 1090 vs, 1011 s, 978 m, 837 s, 797 s, 696 w, 621 m, 552 s, 507 w, 488 w, 465 w. Anal. Calcd. for $C_{96}H_{122}Cl_2Mn_4N_{10}O_{23}Si_6$ (M = 2243.23 g/mol), %: C, 51.4; H, 5.48; N, 6.24. Found: C, 50.97; H, 5.49; N, 6.19. The phase purity of the isolated bulky material was confirmed by the X-ray powder diffraction patterns of compound **1** recorded at room temperature. As shown in Figure S7, the experimental pattern is consistent with the simulation one obtained from the single-crystal diffraction data.

## 4. Conclusions

The synthesis, structure, hydrophobic behavior, surface, thermal, dielectric, and magnetic properties of a new 3D coordination polymer, built from the reaction between 1,3-bis(carboxypropyl)tetramethyldisiloxane, 1,2-di(4-pyridyl)ethylene, and 2,4-lutidine in the presence of $Mn(ClO_4)_2$, have been reported. The single-crystal X-ray diffraction analysis revealed that the 3D coordination polymer has a dense 3D framework structure, as also confirmed by the BET analysis. The hydrophobic character of the studied compound was evidenced by the low sorption capacity, and the integrity of the water drop was maintained while it was rolled on the compound's surface. The polymer demonstrated stability in an inert atmosphere up to 300 °C, with a glass transition at 24 °C. The compound is an electrical insulator, and due to its hydrophobicity, this characteristic is not affected by environmental

humidity. The magnetic results indicated dominant antiferromagnetic interaction along the chain in polymer, evidencing presence of two types of bridging in the chain.

**Supplementary Materials:** The following supporting information can be downloaded at: https://www.mdpi.com/article/10.3390/inorganics11010021/s1. Figure S1: FTIR spectra for Cx, Cx-Na, and polymer **1**. Figure S2: Polymer structure from the perspective of the etdipy moiety (perchlorate counterion and siloxane moiety were omitted for clarity). Figure S3: Polymer structure from the perspective of the siloxane moiety (perchlorate counterion and etdipy moiety were omitted for clarity). Figure S4: Topology of the polymer network. In the topological analysis, the disordered part of the structure was omitted. Figure S5: Dielectric properties of compound **1**, including the relative permittivity ($\varepsilon'$), dielectric loss ($\varepsilon''$), and conductivity ($\sigma$). Figure S6: Magnetization curves versus applied magnetic field for compound **1**. Figure S7: PXRD diffractogram (blue) vs. the one simulated based on single crystal X-ray diffraction data (red). Table S1: Selected bond lengths [Å], angles [°], and hydrogen bonds for compound **1**.

**Author Contributions:** Conceptualization, A.-C.S., M.D. (Mihaela Dascalu), and M.C.; methodology, A.-C.S. and M.D. (Madalin Damoc); software, A.-C.S. and G.N.; validation, S.S. and G.N.; formal analysis, A.-C.S.; investigation, A.-C.S., M.D. (Mihaela Dascalu), and G.N.; resources, M.C.; data curation, A.-C.S.; writing—original draft preparation, M.D. (Mihaela Dascalu) and M.C.; writing—review and editing, A.-C.S., M.D. (Mihaela Dascalu), and M.C.; visualization, S.S.; supervision, M.C.; project administration, M.C.; funding acquisition, M.C. All authors have read and agreed to the published version of the manuscript.

**Funding:** This work was supported by a grant from the Romanian Ministry of Research, Innovation, and Digitization, CNCS—UEFISCDI, project number PN-III-P4-ID-PCE-2020-2000, within PNCDI III, contract 207/2021 (2D-PerMONSil).

**Data Availability Statement:** The data presented in this work are available in the article and Supplementary Materials.

**Acknowledgments:** The authors would like to thank Mihai Asandulesa for the dielectric measurements, Lucian Bahrin for the BET analysis, and Cristian-Dragos Varganici for recording the TGA and DSC curves.

**Conflicts of Interest:** The authors declare no conflict of interest.

## References

1. Du, M.; Li, C.P.; Liu, C.S.; Fang, S.M. Design and construction of coordination polymers with mixed-ligand synthetic strategy. *Coord. Chem. Rev.* **2013**, *257*, 1282–1305. [CrossRef]
2. Li, Z.Y.; Zhang, C.; Zhai, B.; Han, J.C.; Pei, M.C.; Zhang, J.J.; Zhang, F.L.; Li, S.Z.; Cao, G.X. Linking heterometallic Cu–Ln chain units with a 2-methylenesuccinate bridge to form a 2D network exhibiting a large magnetocaloric effect. *CrystEngComm* **2017**, *19*, 2702–2708. [CrossRef]
3. Li, Z.Y.; Zhai, B.; Li, S.Z.; Cao, G.X.; Zhang, F.Q.; Zhang, X.F.; Zhang, F.L.; Zhang, C. Two series of lanthanide coordination polymers with 2-methylenesuccinate: Magnetic refrigerant, slow magnetic relaxation, and luminescence properties. *Cryst. Growth Des.* **2016**, *16*, 4574–4581. [CrossRef]
4. Xiong, W.W.; Miao, J.W.; Ye, K.Q.; Wang, Y.; Liu, B.; Zhang, Q.C. Threading chalcogenide layers with polymer chains. *Angew. Chem. Int. Ed.* **2015**, *54*, 546–550. [CrossRef]
5. Xiong, W.; Zhang, Q. Surfactants as promising media for the preparation of crystalline inorganic materials. *Angew. Chem. Int. Ed.* **2015**, *54*, 11616–11623. [CrossRef]
6. Lu, H.S.; Bai, L.L.; Xiong, W.W.; Li, P.Z.; Ding, J.F.; Zhang, G.D.; Wu, T.; Zhao, Y.L.; Lee, J.M.; Yang, Y.H.; et al. Surfactant media to grow new crystalline cobalt 1,3,5-benzenetricarboxylate metal-organic frameworks. *Inorg. Chem.* **2014**, *53*, 8529–8537. [CrossRef]
7. Xie, Z.; Xu, W.; Cui, X.; Wang, Y. Recent progress in metal-organic frameworks and their derived nanostructures for energy and environmental applications. *ChemSusChem* **2017**, *10*, 1645–1663. [CrossRef]
8. Suh, M.P.; Park, H.J.; Prasad, T.K.; Lim, D.-W. Hydrogen storage in metal-organic frameworks. *Chem. Rev.* **2012**, *112*, 782–835. [CrossRef]
9. Sumida, K.; Rogow, D.L.; Mason, J.A.; McDonald, T.M.; Bloch, E.D.; Herm, Z.R.; Bae, T.H.; Long, J.R. Carbon dioxide capture in metal-organic frameworks. *Chem. Rev.* **2012**, *112*, 724–781. [CrossRef]
10. Halder, G.J.; Kepert, C.J.; Moubaraki, B.; Murray, K.S.; Cashion, J.D. Guest-dependent spin crossover in a nanoporous molecular framework material. *Science* **2002**, *298*, 1762–1765. [CrossRef]
11. Li, J.R.; Sculley, J.; Zhou, H.-C. Metal–organic frameworks for separations. *Chem. Rev.* **2012**, *112*, 869–932. [CrossRef] [PubMed]

12. Yoon, M.; Srirambalaji, R.; Kim, K. Homochiral metal–organic frameworks for asymmetric heterogeneous catalysis. *Chem. Rev.* **2011**, *112*, 1196–1231. [CrossRef] [PubMed]
13. Bartolomé, E.; Alonso, P.J.; Arauzo, A.; Luzón, J.; Bartolomé, J.; Racles, C.; Turta, C. Magnetic properties of the seven-coordinated nanoporous framework material $Co(bpy)_{1.5}(NO_3)_2$ (bpy = 4,4′-bipyridine). *Dalton Trans.* **2012**, *41*, 10382–10389. [CrossRef] [PubMed]
14. Sun, L.; Campbell, M.G.; Dincă, M. Electrically conductive porous metal-organic frameworks. *Angew. Chem. Int. Ed.* **2016**, *55*, 3566–3579. [CrossRef] [PubMed]
15. Zhao, S.-N.; Wang, G.; Poelman, D.; Van Der Voort, P. Luminescent lanthanide MOFs: A unique platform for chemical sensing. *Materials* **2018**, *11*, 572. [CrossRef]
16. Wang, J.; Wang, Y.; Hu, H.; Yang, Q.; Cai, J. From metal-organic frameworks to nanoporous carbons: Recent progress and prospect from energy and environmental perspectives. *Nanoscale* **2020**, *12*, 4238–4268. [CrossRef]
17. Furukawa, H.; Cordova, K.E.; O'Keeffe, M.; Yaghi, O.M. The chemistry and applications of metal-organic frameworks. *Science* **2013**, *341*, 1230444. [CrossRef]
18. Chughtai, A.H.; Ahmad, N.; Younus, H.A.; Laypkov, A.; Verpoort, F. Metal–organic frameworks: Versatile heterogeneous catalysts for efficient catalytic organic transformations. *Chem. Soc. Rev.* **2015**, *44*, 6804–6849. [CrossRef]
19. Hoskins, B.F.; Robson, R. Infinite polymeric frameworks consisting of three dimensionally linked rod-like segments. *J. Am. Chem. Soc.* **1989**, *111*, 5962–5964. [CrossRef]
20. Chakraborty, G.; Park, I.-H.; Medishetty, R.; Vittal, J.J. Two-dimensional metal-organic framework materials: Synthesis, structures, properties and applications. *Chem. Rev.* **2021**, *121*, 3751–3891. [CrossRef]
21. Kostakis, G.E.; Ako, A.M.; Powell, A.K. Structural motifs and topological representation of Mn coordination clusters. *Chem. Soc. Rev.* **2010**, *39*, 2238–2271. [CrossRef] [PubMed]
22. Ako, A.M.; Hewitt, I.J.; Mereacre, V.; Clérac, R.; Wernsdorfer, W.; Anson, C.E.; Powell, A.K. A ferromagnetically coupled $Mn_{19}$ aggregate with a record S = 83/2 ground spin state. *Angew. Chem. Int. Ed.* **2006**, *45*, 4926–4929. [CrossRef] [PubMed]
23. Ma, Y.; Yuan, Y.; Miao, H.; Zhong, Q.; Tang, X.; Cheng, H.; Yuan, R. Structural diversity and magnetic properties of the manganese/carbazol-9-ylpropanate/N,N′-donor reaction system. *Inorganica Chim. Acta* **2015**, *432*, 64–70. [CrossRef]
24. Iikura, H.; Nagata, T. Structural variation in manganase complexes: Synthesis and characterization of manganese complexes from carboxylate-containing chelating ligands. *Inorg. Chem.* **1998**, *37*, 4702–4711. [CrossRef] [PubMed]
25. Albela, B.; Corbella, M.; Ribas, J.; Castro, I.; Sletten, J.; Stoeckli-Evans, H. Synthesis, structural characterization (X-ray and EXAFS), and magnetic properties of polynuclear manganese(II) complexes with chlorobenzoato bridges. *Inorg. Chem.* **1998**, *37*, 788–798. [CrossRef]
26. Lin, Z.-J.; Lü, J.; Hong, M.; Cao, R. Metal–organic frameworks based on flexible ligands (FL-MOFs): Structures and applications. *Chem. Soc. Rev.* **2014**, *43*, 5867–5895. [CrossRef]
27. Pili, S.; Rought, P.; Kolokolov, D.I.; Lin, L.; da Silva, I.; Cheng, Y.; Marsh, C.; Silverwood, I.P.; García Sakai, V.; Li, M.; et al. Enhancement of proton conductivity in non-porous metal-organic frameworks: The role of framework proton density and humidity. *Chem. Mater.* **2018**, *30*, 7593–7602. [CrossRef]
28. Rought, P.; Marsh, C.; Pili, S.; Silverwood, I.P.; Garcia Sakai, V.; Li, M.; Brown, M.S.; Argent, S.P.; Vitorica-Yrezabal, I.; Whitehead, G.; et al. Modulating proton diffusion and conductivity in metal-organic frameworks by incorporation of accessible free carboxylic acid groups. *Chem. Sci.* **2019**, *10*, 1492–1499. [CrossRef]
29. Taksand, K. Exploration of the Ionic Conduction Properties of Porous MOF Materials. Ph.D. Thesis, Université Montpellier, Montpellier, France, 2022.
30. Lim, D.-W.; Kitagawa, H. Proton Transport in Metal–Organic Frameworks. *Chem. Rev.* **2020**, *12*, 8416–8467. [CrossRef]
31. Wang, W.; Yuan, D. Mesoporous carbon originated from non-permanent porous MOFs for gas storage and $CO_2/CH_4$ separation. *Sci. Rep.* **2014**, *4*, 5711. [CrossRef]
32. Aiyappa, H.B.; Pachfule, P.; Banerjee, R.; Kurungot, S. Porous carbons from nonporous mofs: Influence of ligand characteristics on intrinsic properties of end carbon. *Cryst. Growth Des.* **2013**, *13*, 4195–4199. [CrossRef]
33. Zaltariov, M.F.; Cazacu, M.; Sacarescu, L.; Vlad, A.; Novitchi, G.; Train, C.; Shova, S.; Arion, V.B. Oxime-bridged $Mn_6$ clusters inserted in one-dimensional coordination polymer. *Macromolecules* **2016**, *49*, 6163–6172. [CrossRef]
34. Vlad, A.; Cazacu, M.; Zaltariov, M.F.; Bargan, A.; Shova, S.; Turta, C. A 2D metal–organic framework based on dizinc coordination units bridged through both flexible and rigid ligands. *J. Mol. Struct.* **2014**, *1060*, 94–101. [CrossRef]
35. Vlad, A.; Cazacu, M.; Zaltariov, M.F.; Shova, S.; Turta, C.; Airinei, A. Metallopolymeric structures containing highly flexible siloxane sequence. *Polymer* **2013**, *54*, 43–53. [CrossRef]
36. Vlad, A.; Zaltariov, M.F.; Shova, S.; Novitchi, G.; Varganici, C.D.; Train, C.; Cazacu, M. Flexible linkers and dinuclear metallic nodes build up an original metal–organic framework. *CrystEngComm* **2013**, *15*, 5368–5375. [CrossRef]
37. Racles, C.; Shova, S.; Cazacu, M.; Timpu, D. New highly ordered hydrophobic siloxane-based coordination polymers. *Polymer* **2013**, *54*, 6096–6104. [CrossRef]
38. Hoshikawa, R.; Mitsuhashi, R.; Asato, E.; Liu, J.; Sakiyama, H. Structures of dimer-of-dimers type defect cubane tetranuclear copper(II) complexes with novel dinucleating ligands. *Molecules* **2022**, *27*, 576. [CrossRef] [PubMed]
39. Dong, X.; Li, D.; Li, Y.; Sakiyama, H.; Muddassir, M.; Pan, Y.; Srivastava, D.; Kumar, A. A 3,8-connected Cd(II)-based metal-organic framework as an appropriate luminescent sensor for the antibiotic sulfasalazine. *CrystEngComm* **2022**, *24*, 7157–7165. [CrossRef]

40. Blatov, V.A.; Shevchenko, A.P.; Proserpio, D.M. Applied topological analysis of crystal structures with the program package ToposPro. *Cryst. Growth Des.* **2014**, *14*, 3576–3586. [CrossRef]
41. Xue, X.; Wang, J.; Zhu, Q.; Xue, Y.; Liu, H. A two-year water-stable 2D MOF with aqueous NIR photothermal conversion ability. *Dalton Trans.* **2020**, *50*, 1374–1383. [CrossRef]
42. Almenningen, A.; Bastiansen, O.; Ewing, V.; Hedberg, K.; Traetterberg, M. The molecular structure of disiloxane, $(SiH_3)_2O$. *Acta Chem. Scand.* **1963**, *17*, 2455–2460. [CrossRef]
43. Owen, M.J. Why silicones behave funny. *Chim. Nouv.* **2005**, *11*, 1–11.
44. Noll, W. *Chemistry and Technology of Silicones*; Academic Press Inc.: New York, NY, USA, 1968.
45. Voronkov, M.G.; Mileshkevich, V.P.; Yuzhelevskii, Y.A. *The Siloxane Bond: Physical Properties and Chemical Transformations*; Springer: New York, NY, USA, 1978.
46. Hillborg, H.; Tomczak, N.; Olàh, A.; Schönherr, H.; Vancso, G.J. Nanoscale hydrophobic recovery: A chemical force microscopy study of UV/ozone-treated cross-linked poly(dimethylsiloxane). *Langmuir* **2004**, *20*, 785–794. [CrossRef] [PubMed]
47. Gadzikwa, T.; Lu, G.; Stern, C.L.; Wilson, S.R.; Hupp, J.T.; Nguyen, S.B.T. Covalent surface modification of a metal–organic framework: Selective surface engineering via CuI-catalyzed Huisgen cycloaddition. *Chem. Commun.* **2008**, 5493–5495. [CrossRef] [PubMed]
48. Nguyen, J.G.; Cohen, S.M. Moisture-resistant and superhydrophobic metal-organic frameworks obtained via postsynthetic modification. *J. Am. Chem. Soc.* **2010**, *132*, 4560–4561. [CrossRef]
49. Feng, L.; Zhang, Y.; Xi, J.; Zhu, Y.; Wang, N.; Xia, F.; Jiang, L. Petal effect: A Superhydrophobic state with high adhesive force. *Langmuir* **2008**, *24*, 4114–4119. [CrossRef]
50. Bhushan, B.; Nosonovsky, M. The rose petal effect and the modes of superhydrophobicity. *Philos. Trans. R. Soc. A Math. Phys. Eng. Sci.* **2010**, *368*, 4713–4728. [CrossRef]
51. Van der Sman, R.G.M. Predictions of glass transition temperature for hydrogen bonding biomaterials. *J. Phys. Chem. B* **2013**, *117*, 16303–16313. [CrossRef]
52. Murrie, M.; Price, D.J. Molecular Magnetism. *Annu. Rep. Sect. A* **2007**, *103*, 20–38. [CrossRef]
53. Cortés, R.; Drillon, M.; Solans, X.; Lezama, L. Alternating ferromagnetic-antiferromagnetic interactions in a manganese (II)-azido one-dimensional compound: $[Mn(Bipy)(N_3)_2]$. *Inorg. Chem.* **1997**, *36*, 677–683. [CrossRef]
54. Ma, Y.; Zhang, J.Y.; Cheng, A.L.; Sun, Q.; Gao, E.Q.; Liu, C.M. Antiferro- and ferromagnetic interactions in Mn(II), Co(II), and Ni(II) compounds with mixed azide—carboxylate bridges. *Inorg. Chem.* **2009**, *48*, 6142–6151. [CrossRef] [PubMed]
55. Zhang, J.Y.; Liu, C.M.; Zhang, D.Q.; Gao, S.; Zhu, D.B. Spin-canting in a 1D chain Mn(II) complex with alternating double end-on and double end-to-end azido bridging ligands. *Inorg. Chem. Commun.* **2007**, *10*, 897–901. [CrossRef]
56. Zhuang, G.; Li, X.; Wen, Y.; Tian, C.; Gao, E. Structures and magnetic properties of manganese(II) compounds based on chains with simultaneous carboxylate and pseudohalide bridges. *Eur. J. Inorg. Chem.* **2014**, *2014*, 3488–3498. [CrossRef]
57. Durot, S.; Policar, C.; Pelosi, G.; Bisceglie, F.; Mallah, T.; Mahy, J.P. Structural and magnetic properties of carboxylato-bridged manganese(II) complexes involving tetradentate ligands: Discrete complex and 1D polymers. Dependence of J on the nature of the carboxylato bridge. *Inorg. Chem.* **2003**, *42*, 8072–8080. [CrossRef]
58. Gómez, V.; Corbella, M.; Font-Bardia, M.; Calvet, T. A M1,1- or M1,3-carboxylate bridge makes the difference in the magnetic properties of dinuclear MnII compounds. *Dalton Trans.* **2010**, *39*, 11664–11674. [CrossRef]
59. Abu-Youssef, M.A.M.; Escuer, A.; Goher, M.A.S.; Mautner, F.A.; Vicente, R. Structural characterization and magnetic behaviour of the ferro-antiferromagnetic alternating manganese–azido chain $[Mn(3\text{-Et},4\text{-Mepy})_2(\mu\text{-}N_3)_2]_n$ (3-Et,4-Mepy = 3-Ethyl-4-Methylpyridine). *Eur. J. Inorg. Chem.* **1999**, *1999*, 687–691. [CrossRef]
60. Christian, P.; Rajaraman, G.; Harrison, A.; Helliwell, M.; McDouall, J.J.W.; Raftery, J.; Winpenny, R.E.P. Synthesis and studies of a trinuclear Mn(II) carboxylate complex. *Dalton Trans.* **2004**, *16*, 2550–2555. [CrossRef]
61. Rigaku, O.D. *CrysAlisPro Software System*, Version 1.171.38.46; Rigaku Corporation: Oxford, UK, 2015.
62. Dolomanov, O.V.; Bourhis, L.J.; Gildea, R.J.; Howard, J.A.K.; Puschmann, H. OLEX2: A complete structure solution, refinement and analysis program. *J. Appl. Crystallogr.* **2009**, *42*, 339–341. [CrossRef]
63. Sheldrick, G. SHELXT—Integrated space-group and crystal-structure determination. *Acta Crystallogr. Sect. A Found. Adv.* **2015**, *71*, 3–8. [CrossRef]
64. Sheldrick, G. Crystal structure refinement with SHELXL. *Acta Crystallogr. Sect. C Struct. Chem.* **2015**, *71*, 3–8. [CrossRef]
65. Pascal, P. Recherches Magnetochimiques. *Ann. Chim. Phys.* **1910**, *19*, 5–70.